Volume 15, Number 2, 2022. pp. 149-160

Jordan Journal of Physics

ARTICLE

BALQARAD Geant4 Model: Enhancement in γ-ray Spectroscopy and Validation

E. Ababneh[a], **S. Al-Amarat**[a], **S. Okoor**[b] , **M. M. Imran**[a] and **S. Dababneh**[a]

[a] *Department of Physics, Faculty of Science, Al-Balqa Applied University, Salt 19117, Jordan.*

[b] *Physics Department, Yarmouk University, Irbid 21163, Jordan.*

Doi: **https://doi.org/10.47011/15.2.5**

Received on: 12/10/2020; *Accepted on: 12/01/2021*

Abstract: Advances in gamma-ray spectroscopy allow for excellent background suppression and increased efficiency using composite Clover detectors with combinations of active shields. The events from such combinations, registered in list mode and analyzed offline, promote significant sensitivity improvements for gamma detection. This study utilizes the modularity of such composite of high-purity germanium radiation detectors to investigate their applicability in different possible fields. A comprehensive survey is conducted on the appropriate radioactive isotope serving each application. According to its decay scheme, investigation on the proper modes of operation for each isotope is carried out by Monte Carlo simulation applied to the Clover detector geometry. Addback factor measurements were performed using the newly acquired BALQARAD Clover. In an offline analysis through self-developed software, the Clover direct and addback performances are deduced *versus* gamma-ray energy. Measurement results obtained using the Clover detectors agree reasonably well with those obtained by Monte Carlo simulation.

Keywords: Geant4, HPGe, Clover-type detector, Detector modeling and simulation, Modes of operation, Addback factor.

Introduction

While standard gamma-ray spectrometry is commonly used to satisfy various requirements, many significant applications involving highly sensitive detection and gamma-ray measurement are hampered by ambient backgrounds and need enhanced signal-to-background ratios. Therefore, due to crystal size restriction, poor time characteristics and large Doppler broadening of the energy spectrum, standard spectroscopy is not well-suited for such applications. Nowadays, the increasing number of stations around the world for radiation detection equipment, mainly gamma-ray detectors, reflects the public interest in radioactive wastes and other contaminations in the surrounding environment. Recent advances using composite and segmented HPGe Clover detectors as active shields in conjunction with scintillators provide high degrees of versatility for various kinds of ambient, cosmic and sample relevant to background suppression. Besides, attempts to maximize efficiency by measuring at close geometry with standard setups are combined with severe associated effects, like summing, and limiting the measurement's accuracy. Combined with extensive Monte Carlo simulations, the essential corrections due to self-absorption, extended source and true coincidence summing can be reliably obtained, allowing for accurate measurement combined with high efficiency. Therefore, in addition to national security applications, food and water radiological

Corresponding Author: E. Ababneh **Email**: eshraq.ababneh@bau.edu.jo

protection, energy and natural resource applications, many environmental radioactivity measurements are foreseen to benefit from such a sensitive system.

Continued global research dedicated to the detection of low activities and yields by specific gamma signatures is reported in various literature articles [1-5], which revealed steady improvements through the use of arrays of Ge detectors in resolving power, efficiency and high ratio of full-energy to partial-energy events.

Researchers were motivated to investigate further the early encouraging results of using Clover HPGe detectors in several applications and fields. Dababneh *et al.,* (2004) examined the benefits and disadvantages of different modes of operation. An experimental approach for determining the summing correction factor was formulated for the setup of two Clover HPGe detectors of the Karlsruhe Research Center in Germany [6]. Besides, in 2014, Dababneh *et al.,* reported on a setup of Clover HPGe detector in coincidence with specified energy windows in BGO counters covering a large solid angle and combined with large plastic veto counters, which led to a significantly improved sensitivity that allows for clear identification of specific γ-transitions [7]. Different modes of operation have been tested for optimizing the final experimental setup. Sarmiento *et al.* used an experimental setup consisting of composite Ge and strongly segmented Si detectors in 2012 to investigate the nuclear structure of the heaviest elements [8]. A comparison between the simulated detector response of complex decay modes and the experimental data was constructed. A contrast was constructed between the simulated detector response of complex modes of decay and the experimental data [8]. The results provided an excellent testing scenario for new gating and triggering possibilities. Furthermore, a Canberra CryoPulse 5 high-purity germanium (HPGe) semiconductor detector was used to classify and quantify the isotopes that emit gamma in ports and waterways [9]. An experimental setup consisting of 8 segmented Clover HPGe detectors [10] has also investigated collective excitation and single-particle state interaction. For any composite detector, the full detection mode is calculated by simultaneously testing direct and addback modes. The addback mode's advantage arises when the escaped events from one crystal may be recorded in the other crystals. This substantially increases the contribution to the full-energy peak (FEP) efficiency and reduces the Compton continuum [11].

Despite the above research efforts, when complex isotopes are involved in the decay mode or complicated calculation methods, many measurement difficulties can arise. It is worth mentioning here that there is no widely used integrated measurement method with well-defined calculation techniques. This study aims to perform a comprehensive analysis and review of different radioactive elements, analyze the application used and analyze preferable modes of operation based on the isotope decay scheme. This can be carried out with a validated and well-controlled measurement method *via* a newly acquired active shielded Clover detector named BALQARAD Clover, located at Saed Dababneh Laboratory (SDL) for Radiation Measurements at Al-Balqa Applied University in Salt, Jordan. The BALQARAD Clover, to the best of our knowledge, is the first of its kind in the Middle East and in the Arab world. A model was developed by Geant4 code for the Clover and then validated after comparison was performed between experimental and simulated data using various radioactive point sources. Finally, for the BALQARAD Clover, the addition factor as a function of gamma energy was also calculated.

Materials and Methods

Clover Detector Setup

The BALQARAD detection system is a composite detection array consisting of four high-purity germanium crystals of the N-type arranged as Clover-shaped and different scintillator types. Each crystal's size is 60 mm in diameter and 60 mm in length and each crystal has a relative efficiency of 40%. For the BALQARAD Clover, a highly segmented active shield is specifically designed and consists of several BGO ($Bi_4Ge_3O_{12}$) and CsI(TI) scintillators surrounding the Clover (front, side and back scintillators). Large plastic scintillator panels fixed on top, right and left sides of the setup were used to select or reject particular Clover signals according to different criteria, mainly reducing cosmic-ray backgrounds. Each of Ge crystals and active shields provides energy-time information recorded event-by-event in the list file.

Modes of Operation

Different modes of operation are used for counting and analyzing the data. The perfect mode used for sample characterization depends on the decay scheme of the studied nuclide, the energies of gamma being analyzed and other nuclides in the sample that may interfere with the analysis being performed. As a result of the addback mode, events that are registered within a given timing window and then added together are considered. By adding Compton's energies scattered among all the crystals, the full-energy peak is populated by more events and the Compton continuum is reduced. Therefore, less background continuum at low energy will be provided in the spectrum. If two or more photons are emitted simultaneously and detected in separate crystals, the addback mode integrates these energies before binning them into the spectrum. This true coincidence summing is the drawback of using the addback mode. Thus, when studying radionuclides with cascade gammas in the addback mode, careful consideration must be taken. When each of the crystals is treated as a separated detector, then the operation is called direct mode. In this mode, each signal is registered separately and then the number of counts is added together, channel by channel, into the final direct mode spectrum summed up. Due to the solid angle, the direct mode is not oversensitive to true coincidence summing, although Compton's continuum is much higher.

Geant4 Model of the Clover Crystals

Monte Carlo simulation has been conducted to investigate the BALQARAD detection system's characteristics in various operation modes for different isotopes. Therefore, the experimental setup shown in Fig. 1 was modeled using the toolkit Geant4 [12] and extensive simulation runs were performed. The detector's model geometry consisted of the four Ge crystals, the scintillators surrounding them, the front shield of the BGO, the side shield of the BGO and the back catcher of the CsI, as well as the canisters containing these components. The lead shield and the source housings have also been modeled. It is worth mentioning here that the validation of the scintillation detectors output of the BALQARAD system will not be included in the current study.

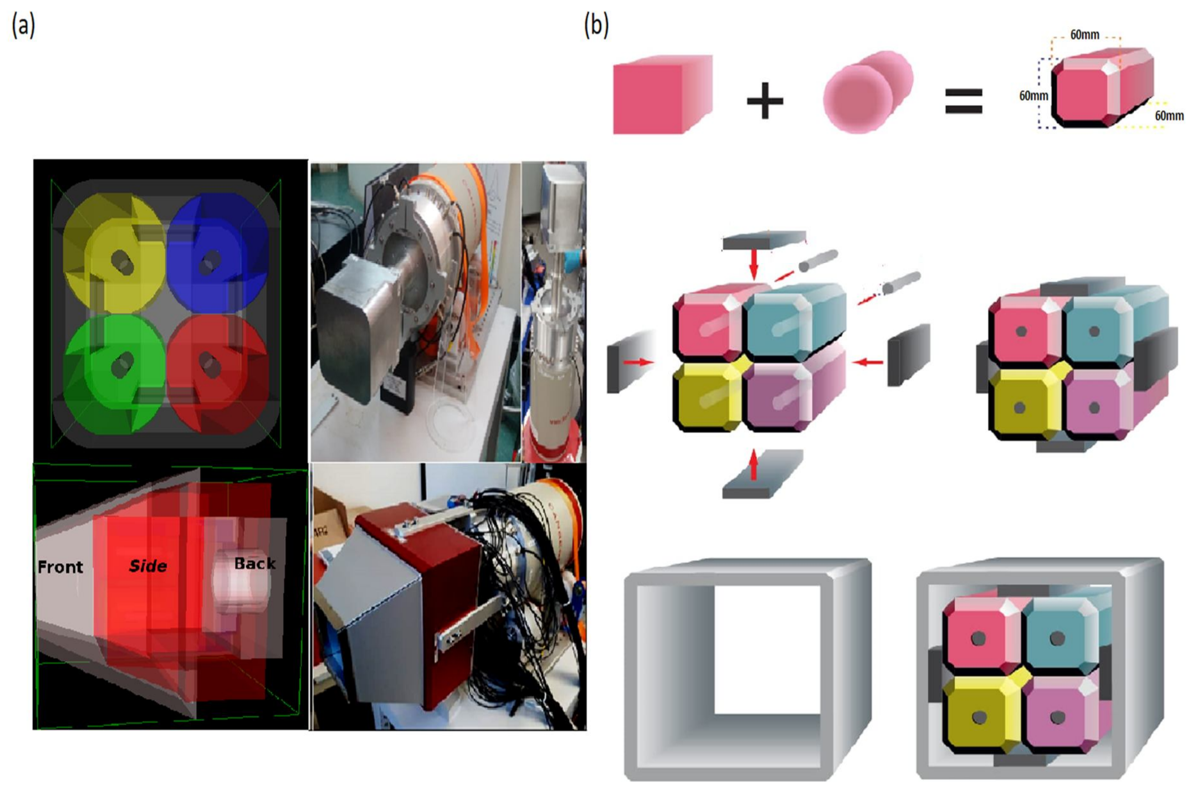

FIG. 1. The BALQARAD active shielded Clover detector at Al-Balqa Applied University in Jordan. (a) Right panel: side pictures of the Clover and the active shield of the system. Left panel: The Monte Carlo model prepared using Geant4 showing the different components of the active shield and the Clover four crystals. (b) Sketch of the Boolean structure of the Clover crystals, which was constructed by detailed Geant4 simulation.

In the design, four germanium crystals were specified; each one was separately identified. Each crystal is a composite of many geometric shapes designed and then fused to obtain the crystal's final shape, as shown in Fig. 1. We first describe the crystal's geometry and construct the physical structure by thorough assignment of its component material, such as density, atomic number and mass number. Finally, the physical and geometrical definitions are linked together and the final crystal coordination is determined in the defined world.

Addback Factor

The addback factor F is defined as the ratio of the FEP detection efficiency of the addback mode to that of the direct mode. Therefore, the addback factor measures the increase in the FEP efficiency for a certain gamma-ray of energy E_γ [11].

Duchene explored the main feature of photopeak detection efficiency in composite detectors such as Clover in 1999 and the findings were contrasted with those obtained by simulation [3]. He found that the fit of the experimental data leads to an expression for the addback factor $F(E_\gamma) = 1 + f(E_\gamma)$, where f is the addition factor that directly depends on the photon energy. The photoelectric effect is dominant at gamma-ray energy below 130 keV. Consequently, the FEP normally does not contribute much to multiple events and both direct and addback modes are the same. The addback factor F is equivalent to 1 ($f = 0$) over an energy range of less than 130 keV. The Compton scattering probability is increased at higher energies (above 130 keV) due to photon scattering in more than one crystal. The addition factor begins to increase with energy, as the addback mode would be more efficient. Therefore, the present work aims to test the BALQARAD device addback factor (F) using several gamma-ray energies obtained from ^{60}Co, ^{137}Cs and ^{22}Na point sources. For this purpose, the Clover's physical model was developed and the additional factor equation was obtained and compared with the simulated one.

Results and Discussion

The geometry was evaluated using a hypothetical Geant4 particle called Geantino (a non-interacting particle), after creating a Monte Carlo code based on comprehensive modeling of the device architecture. To verify the modeled geometry, which was perfectly matched with the real one, the particle-tracking information was used. A special simulation run was also carried out to compare our built code's performance to the experimental measurements.

The Validation of BALQARAD Clover Simulation Model

A comparison was carried out between experimental data and the results obtained from the simulation. In the validation process, several point sources (^{60}Co, ^{137}Cs and ^{22}Na) located at 24 mm from the Clover's front side were used. The source-detector distance used in the validity was settled at 24 cm, typically to avoid high detection dead time. Table 1 shows the full peak net area for the point sources in the addback and direct modes. It is evident that the simulated and measured net areas are in good agreement, with an average error percentage of less than 6%. It is also clear that the addback mode is better than the direct mode for all isotopes due to the high addback efficiency in the full-energy peak on the expense of the corresponding Compton continuum. Measurements of a simple decay scheme, as in ^{137}Cs source with energy 661.65 keV where Compton scattering is the dominant interaction, confirmed the addback gain as illustrated in the gamma-ray spectrum in Fig. 2a. In more complex decay schemes, such as ^{60}Co and ^{22}Na, two full energy peaks appear in coincidence. This will reduce the events recorded at the full-energy peak and cause the summing peak's appearance as shown in ^{60}Co and ^{22}Na gamma-ray spectrum in Fig. 2b and Fig. 2c, respectively. It can be seen that in each spectrum, the addback mode is higher than the direct one. For ^{22}Na, the slight difference between the two modes occurs due to the strong annihilation peak at 511 keV observed in the ^{22}Na isotope. Therefore, the summing peak is considered high in the case of the addback mode, since the full and the annihilation peaks coincide.

TABLE 1. Experimental and simulated full-peak net areas for ^{60}Co, ^{137}Cs and ^{22}Na point sources.

Source		^{137}Cs	^{60}Co		^{22}Na
Energy Peak		661 keV	1173 keV	1332 keV	1274 keV
Direct	Experimental	710057	149040	133963	39020
	Simulation	747316	147298	133168	37360
Percentage error (%)		5%	1%	0.5%	4%
Addback	Experimental	933151	185027	167071	39345
	Simulation	984908	180790	164531	38651
Percentage error (%)		5%	2%	1%	1%

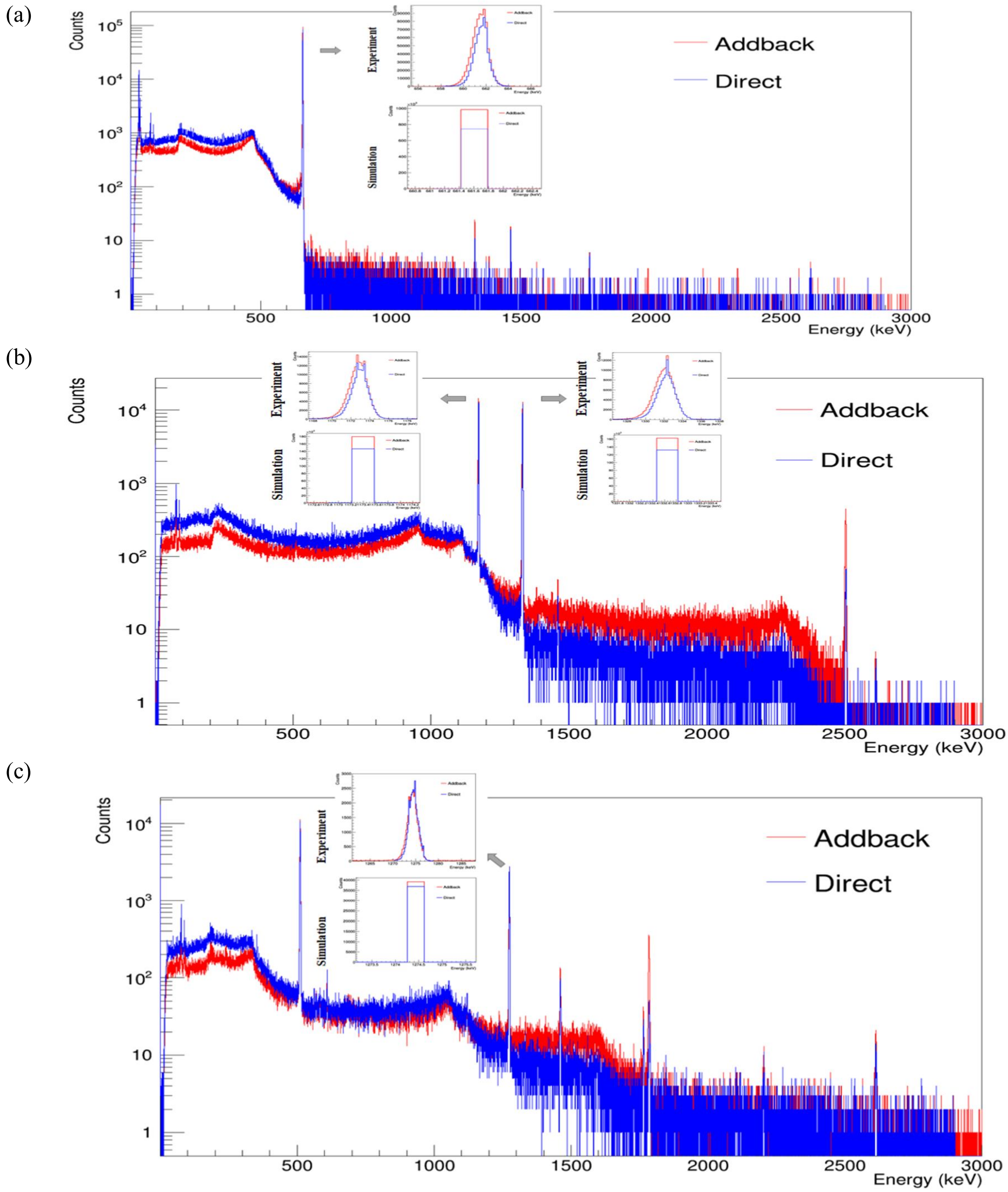

FIG. 2. Gamma-ray spectra in different modes of operation. The observed full peak is compared with the simulated peak; both peaks confirmed the addback gain for (a) ^{137}Cs, (b) ^{60}Co and (c) ^{22}Na; the slight difference between the two modes in ^{22}Na is observed due to the summing peak at 1785 keV as a result of 511 keV and 1274 keV addition.

Simulated Detection Mode for Different Radionuclides

A literature survey shows that, for safety applications, the radiation content of various radiological, environmental, food and water samples has been reviewed. Each application involves measuring a particular radioisotope for a specific sample composition with its decay scheme. All radionuclides of concern in various applications that are part of the pathways leading to internal and external exposure are involved in the summarized survey in Table 2.

The well-validated simulation code was used to run a simulation to determine the radionuclide addback/direct mode in various environmental applications. A separate code written in the ROOT environment [30] is consequently used to finalize the analysis and to evaluate the counts in these two modes. The perfect mode to be used in any sample depends on the decay scheme of the studied nuclide, the energies of gamma that being analyzed and other nuclides in the sample which may interfere with the analysis being performed. One million events at the energies of interest were found to be sufficient to achieve satisfactory statistics. It is well known that photopeak interference occurs in complicated spectra produced from some environmental materials. For example, a typical case is the 186 keV photopeak, generated from the ^{235}U and ^{226}Ra photons of 185.72 keV and 186.25 keV, respectively [31].

TABLE 2. List of radionuclides of interest for different applications.

Application	Radionuclide	References
Water	^{238}U, ^{235}U, ^{226}Ra, ^{232}Th, ^{40}K, ^{137}Cs, ^{228}Ra, ^{222}Rn, ^{210}Po, ^{210}Pb, ^{230}Th, ^{90}Sr, ^{224}Ra, ^{223}Ra	[13-16]
Air	^{3}H, ^{14}C, ^{51}Cr, ^{54}Mn, ^{60}Co, ^{65}Zn, ^{85}Kr, ^{90}Sr, ^{99}Tc, ^{103}Ru, ^{106}Ru, ^{125}Sb, ^{129}I, ^{131}I, ^{137}Cs, ^{144}Ce, ^{154}Eu, ^{155}Eu, ^{234}U, ^{235}U, ^{238}U, ^{238}Pu, ^{239}Pu, ^{240}Pu, ^{241}Am	[17]
Food	^{238}Pu, ^{239}Pu, ^{240}Pu, ^{241}Am, ^{90}Sr, ^{106}Ru, ^{129}I, ^{131}I, ^{235}U, ^{35}S,^{60}Co, ^{89}Sr, ^{103}Ru, ^{134}Cs, ^{137}Cs, ^{144}Ce, ^{192}Ir, ^{3}H, ^{14}C, ^{99}Tc	[18-20]
Soil	^{60}Co, ^{137}Cs, ^{90}Sr, ^{238}Pu, ^{239}Pu, ^{240}Pu, ^{235}U, ^{232}Th, ^{226}Ra, ^{210}Pb, ^{40}K, ^{228}Ac, ^{214}Bi, ^{222}Rn, ^{131}I, ^{134}Cs, ^{129m}Te, ^{95}Nb	[21-23]
Spices	^{226}Ra, ^{232}Th, ^{40}K	[24]
Brazil nuts	^{222}Ra, ^{224}Ra, ^{226}Ra	[25]
Coal	^{238}U, ^{226}Ra, ^{210}Po, ^{210}Pb, ^{232}Th, ^{228}Ra, ^{40}K	[26]
Oil and gas	^{238}U, ^{226}Ra, ^{210}Po, ^{210}Pb, ^{222}Rn, ^{232}Th, ^{228}Ra, ^{224}Ra	[26]
Phosphate rocks	^{238}U, ^{232}Th, ^{226}Ra, ^{228}Ra, ^{40}K	[26]
Fertilizer production	^{238}U, ^{232}Th, ^{226}Ra	[26]
Building materials	^{226}Ra, ^{232}Th, ^{40}K	[27,28]
Rare metals	^{238}U, ^{232}Th, ^{40}K	[29]

However, the use of the Clover system allows for identifying such events in terms of direct and addback modes with high sensitivity. Table 3 summarizes the isotopes of interest in the environmental applications, the counts in both direct and addback modes for each isotope's full-energy peaks, and finally, the preferred operation mode for each isotope due to the complexity of the decay scheme. For gamma emitters of low-energy range (less than 130 keV) such as ^{129}I, which has a simple decay scheme and emitting gamma-ray of energy ≈ 39.5 keV, the direct mode and addback mode are the same and appear to be in harmony at low-energy region due to the dominance of photoelectric effect. The behavior in the addback mode is better than in the direct mode because of the superiority of the Compton effect for higher energies (above 130 keV), as in the case of ^{40}K with a simple decay scheme characterized by its dominant gamma line at 1460.820 keV with 10.66% relative intensity.

TABLE 3. The simulated peak net area recorded by addback and direct modes for isotopes that may be used in different applications.

Nuclide		Gamma energy (keV)	Intensity (%)	Direct net area	Addback net area	Preferred operation mode
^{238}U	^{234}Th	63.29	3.7	95260	66151	Direct
	^{214}Bi	609.320	45.49	239382	221785	Direct
	^{214}Bi	768.360	4.894	20639	18873	Direct
	^{214}Bi	934.056	3.107	11394	10752	Direct
	^{214}Bi	1120.294	14.92	47450	47290	Both
	^{214}Bi	1238.122	5.834	16889	16832	Both
	^{214}Bi	1377.669	3.988	11384	14364	Addback
	^{214}Bi	1407.988	2.394	5899	5968	Addback
	^{214}Bi	1509.210	2.130	5361	5698	Addback
	^{214}Bi	1729.595	2.878	7616	12851	Addback
	^{214}Bi	1764.491	15.30	35503	42286	Addback
	^{214}Bi	1847.429	2.025	4872	7215	Addback
	^{214}Bi	2204.059	4.924	9354	11432	Addback
^{226}Ra	^{226}Ra	186.211	3.64	50366	38219	Direct
	^{214}Pb	241.9950	7.251	91381	81017	Direct
	^{214}Pb	295.2228	18.42	197532	185453	Direct
	^{214}Pb	351.9321	35.60	327074	314925	Direct
	^{214}Bi	609.320	45.49	244968	239571	Direct
	^{214}Bi	768.360	4.894	20603	20066	Both
	^{214}Bi	934.056	3.107	11593	11574	Both
	^{214}Bi	1120.294	14.92	48827	51226	Addback
	^{214}Bi	1238.122	5.834	17240	18200	Addback
	^{214}Bi	1377.669	3.988	11675	15311	Addback
	^{214}Bi	1407.988	2.394	5890	6240	Addback
	^{214}Bi	1509.210	2.130	5602	6139	Addback
	^{214}Bi	1729.595	2.878	7642	13943	Addback
	^{214}Bi	1764.491	15.30	35631	45263	Addback
	^{214}Bi	1847.429	2.025	5016	7759	Addback
	^{214}Bi	2204.059	4.924	9752	12616	Addback
^{232}Th	^{228}Ac	129.065	2.42	46973	30801	Direct
	^{228}Ac	209.253	3.89	60827	47027	Direct
	^{212}Pb	238.632	43.6	516350	411188	Direct
	^{228}Ac	270.245	3.46	48365	36452	Direct
	^{228}Ac	328.000	2.95	37135	29168	Direct
	^{228}Ac	338.320	11.27	113876	102628	Direct
	^{228}Ac	463.004	4.40	29916	24927	Direct
	^{212}Bi	727.330	6.67	30177	28729	Direct
	^{228}Ac	794.947	4.25	19723	17478	Direct
	^{228}Ac	911.204	25.8	94982	99604	Addback
	^{228}Ac	964.766	4.99	18318	18685	Both
	^{228}Ac	968.971	15.8	54711	57703	Addback
	^{228}Ac	1588.20	3.22	8060	9305	Addback
------	^{40}K	1460.820	10.66	30356	43364	Addback
------	^{137}Cs	661.657	85.10	466011	614233	Addback
------	^{210}Pb	46.539	4.25	83107	83573	Both
------	^{224}Ra	240.986	4.10	50129	44752	Direct
------	^{223}Ra	144.235	3.27	63108	60106	Direct
	^{223}Ra	154.208	5.70	106522	102944	Direct

Nuclide		Gamma energy (keV)	Intensity (%)	Direct net area	Addback net area	Preferred operation mode
	^{223}Ra	269.463	13.9	159912	168859	Addback
	^{223}Ra	323.871	3.99	34906	38125	Addback
	^{223}Ra	338.282	2.84	23974	26526	Addback
------	^{51}Cr	320.0824	9.910	104427	123046	Addback
------	^{54}Mn	834.848	99.9760	453507	614488	Addback
------	^{60}Co	1173.228	99.85	329146	404409	Addback
	^{60}Co	1332.492	99.9826	297208	366926	Addback
------	^{65}Zn	1115.539	50.04	182279	253582	Addback
------	^{85}Kr	513.997	0.434	2889	3741	Addback
------	^{103}Ru	497.085	91.0	640853	810077	Addback
	^{103}Ru	610.333	5.76	33602	44224	Addback
------	^{125}Sb	176.314	6.84	110480	106298	Direct
	^{125}Sb	427.874	29.6	237780	291185	Addback
	^{125}Sb	463.365	10.49	79268	101993	Addback
	^{125}Sb	600.597	17.65	104273	135082	Addback
	^{125}Sb	606.713	4.98	29377	37962	Addback
	^{125}Sb	635.950	11.22	63330	84218	Addback
------	^{129}I	39.578	7.51	143884	145440	Both
------	^{131}I	80.185	2.62	58006	48723	Direct
	^{131}I	284.305	6.12	69965	74362	Addback
	^{131}I	364.489	81.5	757827	918408	Addback
	^{131}I	636.989	7.16	40545	53346	Addback
------	^{144}Ce	133.515	11.09	216271	207295	Direct
------	^{154}Eu	123.0706	40.4	790576	687963	Direct
	^{154}Eu	247.9290	6.89	81733	68840	Direct
	^{154}Eu	591.755	4.95	27690	27563	both
	^{154}Eu	723.3014	20.06	95466	104538	Addback
	^{154}Eu	756.8020	4.52	19849	19350	Direct
	^{154}Eu	873.1834	12.08	50387	54728	Addback
	^{154}Eu	996.29	10.48	43048	56802	Addback
	^{154}Eu	1004.76	18.01	65759	81286	Addback
	^{154}Eu	1274.429	34.8	109927	139796	Addback
------	^{155}Eu	86.5479	30.7	703934	711483	Addback
	^{155}Eu	105.3083	21.1	465286	473785	Addback
------	^{234}U	53.20	0.1230	25146	18045	Direct
------	^{241}Am	59.5409	35.9	1032390	734439	Direct
------	^{134}Cs	563.246	8.338	48301	45903	Direct
	^{134}Cs	569.331	15.373	86988	82722	Direct
	^{134}Cs	604.721	97.62	539785	586465	Addback
	^{134}Cs	795.864	85.46	377127	424450	Addback
	^{134}Cs	801.953	8.688	36859	37773	Addback
	^{134}Cs	1365.185	3.017	10372	19894	Addback
------	^{192}Ir	295.9565	28.71	290490	241766	Direct
	^{192}Ir	308.4550	29.70	291476	251717	Direct
	^{192}Ir	316.5061	82.86	813063	769592	Direct
	^{192}Ir	468.0688	47.84	333895	354465	Addback
	^{192}Ir	588.5810	4.522	24581	23995	Direct
	^{192}Ir	604.411	8.216	52665	81939	Addback
	^{192}Ir	612.426	5.34	37139	67763	Addback
------	^{228}Ac	129.065	2.42	46722	30574	Direct
	^{228}Ac	209.253	3.89	60353	46628	Direct

Nuclide		Gamma energy (keV)	Intensity (%)	Direct net area	Addback net area	Preferred operation mode
	^{228}Ac	270.245	3.46	48997	36966	Direct
	^{228}Ac	328.000	2.95	37440	29227	Direct
	^{228}Ac	338.320	11.2	113617	102526	Direct
	^{228}Ac	463.004	4.40	30008	24968	Direct
	^{228}Ac	794.947	4.25	19237	17154	Direct
	^{228}Ac	911.204	25.8	95052	100085	Addback
	^{228}Ac	964.766	4.99	18510	18724	Both
	^{228}Ac	968.971	15.8	54594	57456	Addback
	^{214}Bi	609.320	45.49	256754	284582	Addback
	^{214}Bi	768.360	4.894	21747	23831	Addback
	^{214}Bi	934.056	3.107	11764	13323	Addback
	^{214}Bi	1120.294	14.92	51117	59571	Addback
	^{214}Bi	1238.122	5.834	18278	21672	Addback
	^{214}Bi	1377.669	3.988	12175	17988	Addback
------	^{214}Bi	1407.988	2.394	6206	7390	Addback
	^{214}Bi	1509.210	2.130	5895	7205	Addback
	^{214}Bi	1729.595	2.878	8037	15795	Addback
	^{214}Bi	1764.491	15.30	37576	53803	Addback
	^{214}Bi	1847.429	2.025	5240	9233	Addback
	^{214}Bi	2204.059	4.924	10140	14795	Addback
------	^{129m}Te	459.60	7.7	57422	69809	Addback
	^{129m}Te	487.39	1.42	10532	14276	Addback
------	^{95}Nb	765.803	99.808	484958	651595	Addback
------	^{228}Ra	13.52	1.60	3097	1663	Direct
------	^{222}Ra	324.31	2.77	28457	33224	Addback

However, for radionuclides with complex decay schemes such as ^{228}Ac and ^{214}Bi (Fig. 3 depicts the simulated complex decay schemes of ^{214}Bi), which are the decay products of natural radioactive decay chains, it is observed from the simulation spectra that the addback mode is poor due to coincidence summing. The secular equilibrium occurs in a radioactive decay chain when the daughter's half-life is much shorter than that of the parent radionuclide. In this situation, the parent's decay rate and the production rate of the daughter are approximately constant.

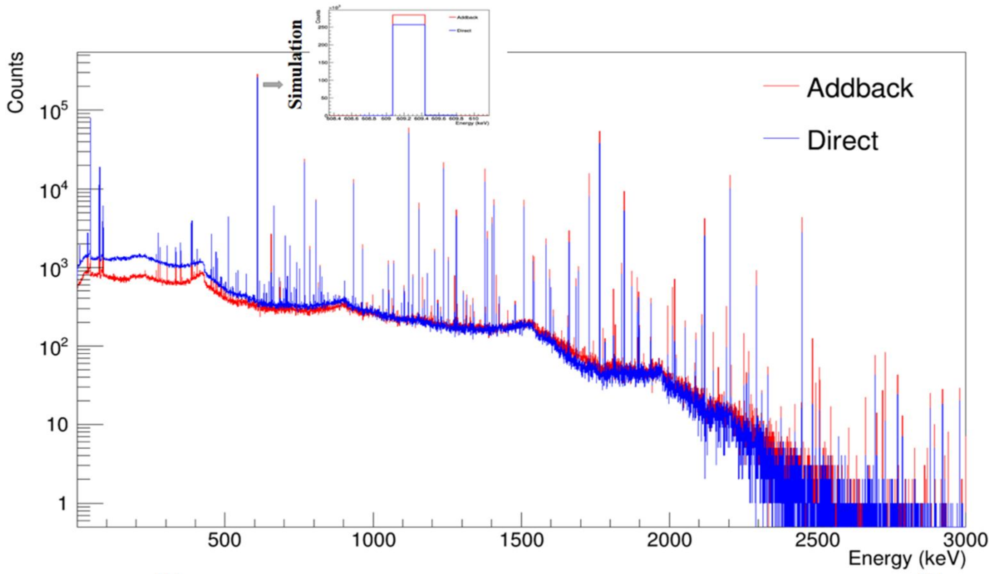

FIG. 3. Simulated ^{214}Bi gamma-ray spectra for both addback and direct modes, where the ^{214}Bi dominant gamma line is at 609.32 keV with 45.49 % relative intensity.

Addback Factor

The addition factor (f) has been performed after measuring the addback factor (F) over different gamma energies obtained from ^{60}Co, ^{137}Cs and ^{133}Ba point sources. The acquired experimental data was fitted to get an equation compared to the simulated one given in Table 4 and Fig. 4a. The ratio is approximately one, because the Compton scattering is very low at lower energies. With the increase in gamma-ray radiation, the addback factor begins to rise, so Compton's scattering becomes more probable. The addback factor becomes almost constant at very high energy, although the likelihood of scattering is still dominant compared with photoelectric absorption in the second crystal.

TABLE 4. The simulated addition factors for several gamma energies compared with those obtained from the experimental results.

Energy (keV)	Addition factor f (Experimental)	Addition factor f (Simulated)
356	0.10773±0.0029	0.12060±0.00318
661	0.2544±0.00355	0.25576±0.00381
1173	0.30734±0.00306	0.30172±0.00305
1332	0.32484±0.00319	0.31388±0.00322

The fitted addition factor equation is expressed, according to Duchene (1999), by the relationship with E_γ in keV [3]:

$$f(E_\gamma) = \begin{cases} P_1 + P_2 \ln E_\gamma , E_\gamma > 130\ keV \\ 0, E_\gamma \le 130\ keV. \end{cases} \quad (1)$$

The fitting parameters of the experimental results acquired from BALQARAD Clover were P_1 = -0.83052 and P_2 = 0.16172. The experimental values are comparable with the simulated full geometry performance, with P_1= -0.77315 and P_2 = 0.15276 fitting parameters (compare two datasets in Fig. 4a and Fig. 4b). The two datasets exhibit the same behavior as predicted and provide a strong agreement between the established Clover model and the actual experiment with satisfactory evidence. After the validation of the Clover simulation code, it is possible now to adopt the code and run the simulation with isotopes of wide energy range such as; ^{133}Ba (356.01 keV with 62.05%), ^{134}Cs (604.72 keV with 97.62%, 569.33 keV with 15.4% and 795.86 keV with 85.5%), ^{137}Cs (661.66 keV with 85.1%), ^{88}Y (898.04 keV with 93.7% and 1836.06 with 99.2%) and ^{60}Co (1173 keV with 99.85% and 1332.49 keV with 99.98%). The new fitting parameters for simulated addback factor with different isotopes with wide energy range are shown in Fig. 4c.

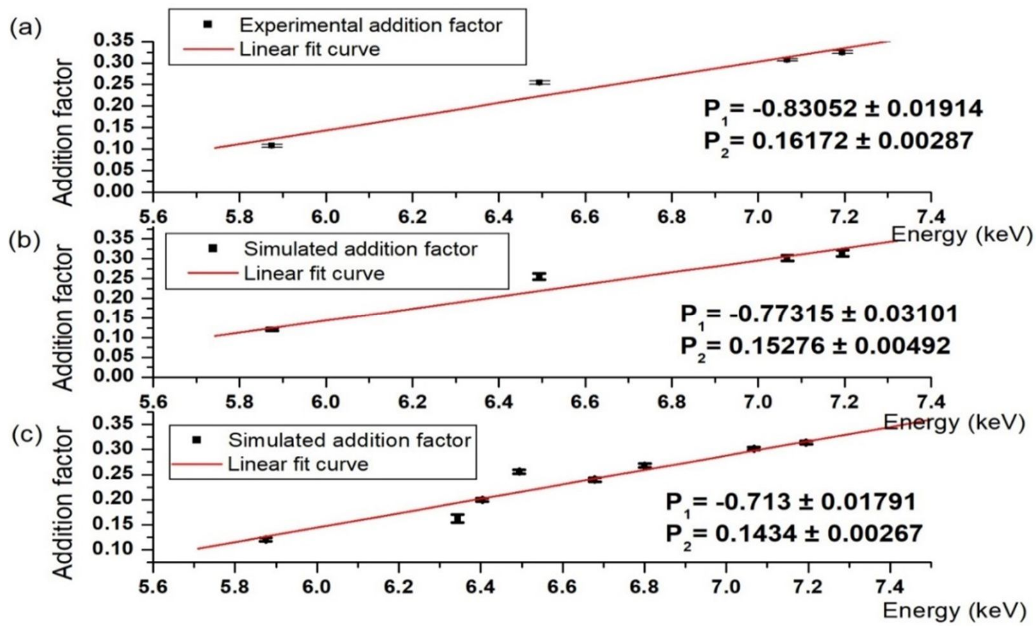

FIG. 4. The linear fit for (a) experimental and (b) simulated addition factors for available radionuclides in the radiation lab. (c) The linear fit for the simulated addition factor for a set of isotopes with a wide range of energy.

Conclusions

To examine possible applications, we have used the modularity of composite HPGe radiation detectors. Comprehensive Monte Carlo simulations based on detailed modeling of the system geometry were performed and compared with the obtained data experimentally. After using the Geant4 model, the results have shown that it is a highly valuable tool for simulating the HPGe system response. The measured addback factor $F(E_\gamma)$ is larger than or equal to one. The measured addition factor has underlined strong agreement between the two sets of data by using experimental and simulated data. For each application, a detailed survey was performed on the appropriate radioactive isotope and the desired operating mode of the Clover detector was determined. Further research into the perception of regional patterns in radionuclides is inspired by the early promising results of using Clover HPGe detectors in many applications and fields.

Acknowledgments

BALQARAD project is supported by the Jordanian Scientific Research Support Fund (SRSF) under grant #Bas/2/4/2014. The authors would like to acknowledge and appreciate the support given by the late BALQARAD founder, Prof. S. Dababneh.

References

[1] Saha Sarkar, M., Datta, P., Ray, I., Deya, C.C., Chattopadhyay, S., Goswami, A., Banerjee, P., Singh, R.P., Joshi, P.K., Paul, S.D., Bhattacharya, S., Bhowmik, R., Chatterjee, J.M., Jain, H.C., Sen, S. and Dasmahapatra, B., Nucl. Instr. and Meth. A, 491 (2002) 113.

[2] Eberth, J. and Simpson, J., Prog. Part. Nucl. Phys., 60 (2008) 283.

[3] Duchêne, G., Beck, F.A., Twin, P.J., De France, G., Curien, D., Han, L., Beausang, W.C., Bentley, A.M., Nolan, J.P. and Simpson, J., Nucl. Instr. and Meth. A, 432 (1999) 90.

[4] Boynton, V.W., Feldman, C.W., Squyres, W.S. *et al.,* Science, 297 (2002) 81.

[5] Horne, M.S., Ph.D. Thesis, The University of Texas at Austin, (2013), USA. http://hdl.handle.net/2152/21557.

[6] Dababneh, S., Patronis, N., Assimakopoulos, A.P., Görres, J., Heil, M., Käppeler, F., Karamanis, D., O'Brien, S. and Reifarth, R., Nucl. Instr. and Meth. A, 517 (2004) 230.

[7] Dababneh, S., Görres, J., Heil, M., Käppeler, F., Reifarth, R. and Wiescher, M., Nucl. Instr. and Meth. A, 737 (2014) 135.

[8] Sarmiento, L.G., Andersson, L.L. and Rudolph, D., Nucl. Instr. and Meth. A, 667 (2012) 26.

[9] Chick, D.M., Master Thesis, Western Kentucky University, (2016), Kentucky. https://digitalcommons.wku.edu/theses/1744.

[10] Belvito, B., Master Thesis, University of Milano, (2015), Italy. http://www.infn.it/thesis/PDF/getfile.php?filename=10181-Belvito-magistrale.pdf.

[11] Rizwan, U.,Garnsworthy, B.A., Andreoiu, C. *et al.,* Nucl. Instr. and Meth. A, 820 (2011) 126.

[12] Geant4. https://geant4.web.cern.ch. Accessed on 20 April 2019.

[13] World Health Organization (WHO), "Guidelines for Drinking-water Quality", Third Edition, (2008). https://www.who.int/water_sanitation_health/publications/gdwq3rev/en/.

[14] Milvy, P. and Cothern, R.C., Environ. Geochem. Health, 11 (1989) 63.

[15] Munter, R., Proc. Estonian Acad. Sci., 62 (2013) 122.

[16] Ahmed, K.N. and Turkish J., Eng. Env. Sci., 28 (2004) 345.

[17] Fritz, G.B. and Patton W.G., Radionuclide Concentrations in Air on the Hanford Site (No. PNNL-13909), A Ten-year Trend Report 1991 through 2000, Pacific Northwest National Lab (PNNL), United States, (2002).

[18] World Health Organization (WHO), Nuclear accidents and radioactive contamination of foods (2011). https://www.who.int/foodsafety/fs_management/radionuclides_and_food_300311.pdf.

[19] Codex Alimentarius Commission (CAC), Fact Sheet on Codex Guideline Levels for Radionuclides in Foods Contaminated Following a Nuclear or Radiological Emergency, (2011). http://www.fao.org/fileadmin/user_upload/agns/pdf/codex_guideline_for_radionuclitide_contaminated_food.pdf.

[20] US Food and Drug Administration (FDA), Supporting document for guidance levels for radionuclides in domestic and imported foods, (2004). https://www.fda.gov/food/chemicals/supporting-document-guidance-levels-radionuclides-domestic-and-imported-foods

[21] Simmons, A.M., Poston, M.T., Fritz, G.B. and Bisping, E.L., Radionuclide Concentrations in Terrestrial Vegetation and Soil Samples on and around the Hanford Site, 1971 through 2008 (PNNL-20577). Pacific Northwest National Lab, United States, (2011).https://www.pnnl.gov/main/publications/external/technical_reports/PNNL-20577.pdf.

[22] Maphoto, P.K., Ph. D. Thesis, University of the Western Cape, (2004). http://hdl.handle.net/11394/1462.

[23] Pallavicini, N., Master Thesis, Swedish University of Agricultural Sciences, Department of Soil and Environment, (2011). https://stud.epsilon.slu.se/3703/2/pallavicini_n_111215.pdf.

[24] Amin, M.R. and Ahmed, F., Pelagia Research Library Advances in Applied Science Research, 4 (2013) 350.

[25] Martins, M., Pacheco, M.A., Lucas, S.C.A., Andrello, C.A., Appoloni, R.C. and Xavier, M.J.J., Acta Amazonica, 42 (2012) 157.

[26] World Nuclear Association, Naturally Occurring Radioactive Materials (NORM). http://www.world-nuclear.org/information-library/safety-and-security/radiation-and-health/naturally-occurring-radioactive-materials-norm.aspxx. Accessed on 01 April 2019.

[27] Quintana, B., Pedrosa, C.M., Vázquez-Canelas, L., Santamaría, R., Sanjuán, A.M. and Puertas, F., Radiat. Isot., 134 (2018) 470.

[28] Ahmed, H.A., Jafir, O.A. and Abdullah, M.H., Jordan J. Phys., 13 (1) (2020) 73.

[29] Shives, K.B.R., British Columbia Geological Survey Paper, 3 (2015) 199.

[30] Brun, R. and Rademakers, F., Nucl. Instr. and Meth. A, 389 (1997) 81.

[31] Anagnostakis, J.M., Radiat. Phys. Chem., 116 (2015) 3.